Supporting Information for "Equatorial Pacific pCO_2 Interannual Variability in CMIP6 Models"

Suki C. K. Wong[1], Galen A. McKinley[1], Richard Seager[1]

[1]Lamont-Doherty Earth Observatory, Columbia University, Palisades, New York

Contents of this file

1. Tables S1 to S2
2. Figures S3 to S9

Corresponding author: Suki C. K. Wong, Lamont-Doherty Earth Observatory, Columbia University, Palisades, New York. (suki.wong@columbia.edu)

October 12, 2022, 8:01pm

Table S1. The CMIP6 models and the ensemble members used in this assessment. The members in bold were the members used to represent the model whenever a single member was used in a calculation or plot.

Models	Member IDs
ACCESS-ESM1-5	**r1i1p1f1**, r2i1p1f1, r3i1p1f1, r4i1p1f1, r5i1p1f1, r6i1p11f1, r8i1p1f1
CanESM5	**r1i1p1f1**, r2i1p1f1, r3i1p1f1, r4i1p1f1, r5i1p1f1, r6i1p11f1, r7i1p1f1, r8i1p1f1,r9i1p1f1, r10i1p1f1, r11i1p1f1, r12i1p1f1, r13i1p1f1, r14i1p1f1, r15i1p1f1, r16i1p1f1, r17i1p1f1, r18i1p1f1, r19i1p1f1, r20i1p1f1, r21i1p1f1, r22i1p1f1, r23i1p1f1, r24i1p1f1, r25i1p1f1, r1i1p2f1, r2i1p2f1, r3i1p2f1, r4i1p2f1, r5i1p2f1, r6i1p2f1, r7i1p2f1, r8i1p2f1, r9i1p2f1, r10i1p2f1
CanESM5-CanOE	**r1i1p1f1**, r2i1p1f1,r3i1p1f1
CESM2	**r1i1p1f1**, r2i1p1f1, r3i1p1f1, r4i1p1f1, r5i1p1f1, r6i1p1f1, r7i1p1f1, r8i1p1f1, r9i1p1f1, r10i1p1f1
CESM2-FV2	**r1i1p1f1**, r2i1p1f1,r3i1p1f1
CESM2-WACCM	**r1i1p1f1**, r2i1p1f1,r3i1p1f1
CESM2-WACCM-FV2	**r1i1p1f1**, r2i1p1f1,r3i1p1f1
CNRM-ESM2-1	**r1i1p1f2**, r2i1p1f2, r3i1p1f2, r4i1p1f2, r5i1p1f2, r6i1p1f2, r7i1p1f2, r8i1p1f2, r9i1p1f2, r10i1p1f2, r11i1p1f2
GFDL-CM4	**r1i1p1f1**
IPSL-CM6A-LR	**r1i1p1f1**, r2i1p1f1, r3i1p1f1, r4i1p1f1, r5i1p1f1, r6i1p1f1, r7i1p1f1, r8i1p1f1, r9i1p1f1, r10i1p1f1, r11i1p1f1, r12i1p1f1, r13i1p1f1, r14i1p1f1, r15i1p1f1, r16i1p1f1, r17i1p1f1, r18i1p1f1, r19i1p1f1, r20i1p1f1, r21i1p1f1, r22i1p1f1, r23i1p1f1, r24i1p1f1, r25i1p1f1, r26i1p1f1, r27i1p1f1, r28i1p1f1, r29i1p1f1, r30i1p1f1, r31i1p1f1, r32i1p1f1
MIROC-ES2L	**r1i1p1f2**, r2i1p1f2, r3i1p1f2, r4i1p1f2, r5i1p1f2, r6i1p1f2, r7i1p1f2, r8i1p1f2, r9i1p1f2, r10i1p1f2
MRI-ESM2-0	**r1i2p1f1**
MPI-ESM1-2-LR	**r1i1p1f1**, r2i1p1f1, r3i1p1f1, r4i1p1f1, r5i1p1f1, r6i1p1f1, r7i1p1f1, r8i1p1f1, r9i1p1f1, r10i1p1f1
MPI-ESM1-2-HR	**r1i1p1f1**, r2i1p1f1, r3i1p1f1, r4i1p1f1, r5i1p1f1, r6i1p1f1, r7i1p1f1, r8i1p1f1, r9i1p1f1, r10i1p1f1
MPI-ESM-1-2-HAM	**r1i1p1f1**, r2i1p1f1
NorESM2-LM	**r1i1p1f1**, r2i1p1f1,r3i1p1f1
NorESM2-MM	**r1i1p1f1**, r2i1p1f1,r3i1p1f1
UKESM1-0-LL	**r1i1p1f2**, r2i1p1f2, r3i1p1f2, r4i1p1f2, r5i1p1f3, r6i1p1f3, r7i1p1f3, r8i1p1f2, r9i1p1f2, r10i1p1f2, r11i1p1f2, r12i1p1f2, r16i1p1f2, r17i1p1f2, r18i1p1f2, r19i1p1f2

Table S2. One standard deviation of each Reynold's decomposition term relative to the time-tendency of $pCO_{2,nonT}$ in models. Values were calculated from a single member run from each model. * The first row shows only the ratio for the second Reynold's term, calculated from a combination of the observations-based products (SeaFlux, ORAS5 and GLODAP). The last column shows the correlation coefficient (r) between $w_{50}\partial_z DIC$ and $pCO_{2,nonT}$ variability.

Models*	$\frac{\sigma(\overline{w_{50}}\partial_z DIC')}{\sigma(\partial_t pCO'_{2,nonT})}$	$\frac{\sigma(w'_{50}\partial_z \overline{DIC})}{\sigma(\partial_t pCO'_{2,nonT})}$	$\frac{\sigma(w'_{50}\partial_z DIC')}{\sigma(\partial_t pCO'_{2,nonT})}$	$\frac{\sigma(w_{50}\partial_z DIC)}{\sigma(\partial_t pCO'_{2,nonT})}$	r
obs-based products	-	4.04	-	-	-
CanESM5	1.91	2.50	1.22	3.51	0.51
CESM2	2.65	2.77	0.96	4.92	0.70
CESM2-FV2	2.08	1.99	0.92	3.72	0.66
CESM2-WACCM	2.67	2.94	0.87	4.91	0.67
CESM2-WACCM-FV2	1.87	2.55	0.82	3.82	0.58
CNRM-ESM2-1	2.03	2.30	1.01	3.59	0.47
GFDL-CM4	1.90	3.16	0.89	4.45	0.63
MIROC-ES2L	2.64	2.17	1.73	3.33	0.31
MRI-ESM2-0	1.96	2.26	0.95	3.79	0.51
NorESM2-LM	1.36	2.03	1.09	2.94	0.51
NorESM2-MM	2.06	2.30	1.26	3.38	0.51
UKESM1-0-LL	2.09	4.11	1.47	5.55	0.54

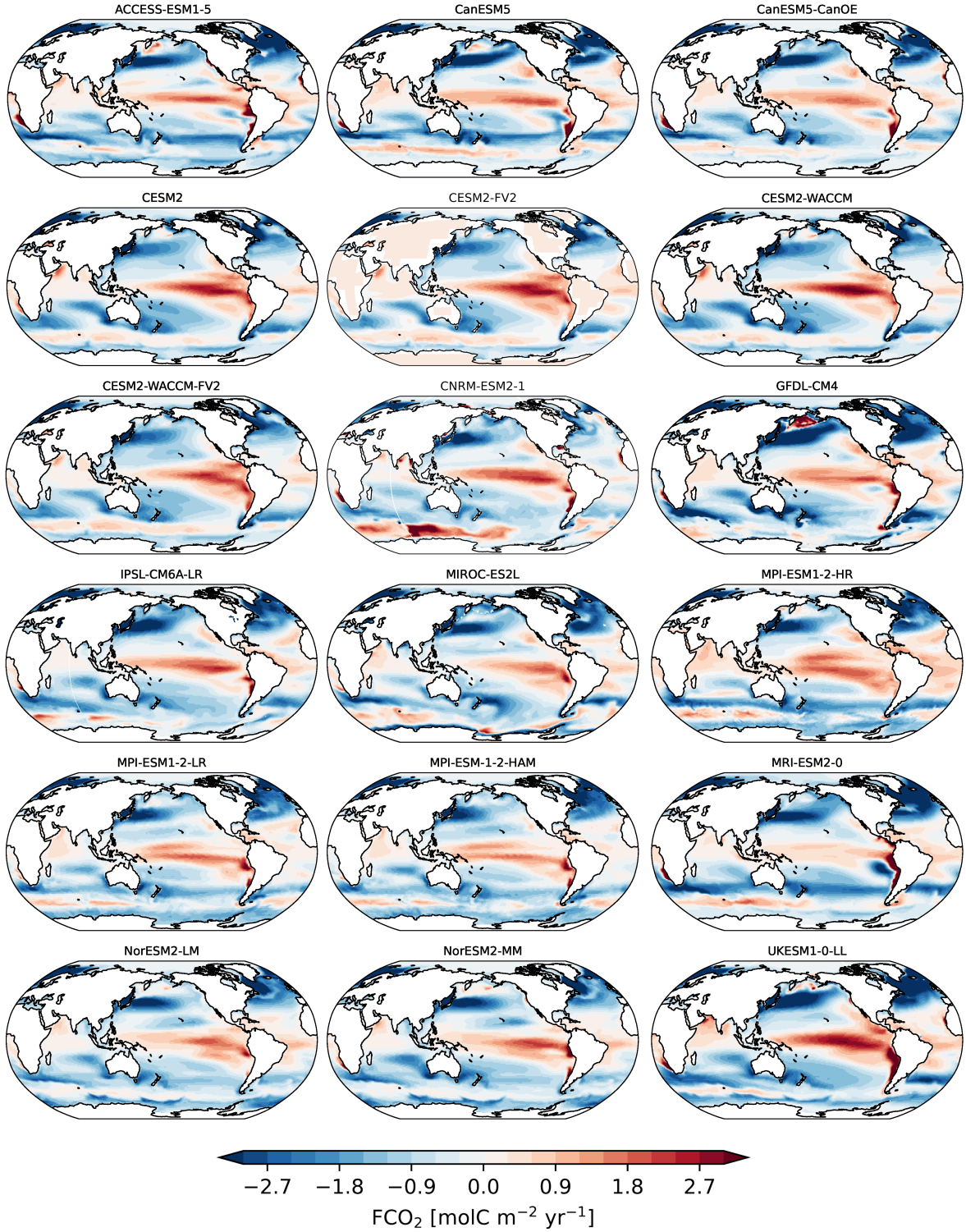

Figure S1. Multiyear mean maps of air-sea CO_2 flux (FCO_2 units: molC m^{-2} yr^{-1} taken over 1990-2014 for 18 CMIP6 models (one member was chosen per model). Positive values (red) represent fluxes from the ocean to the atmosphere.

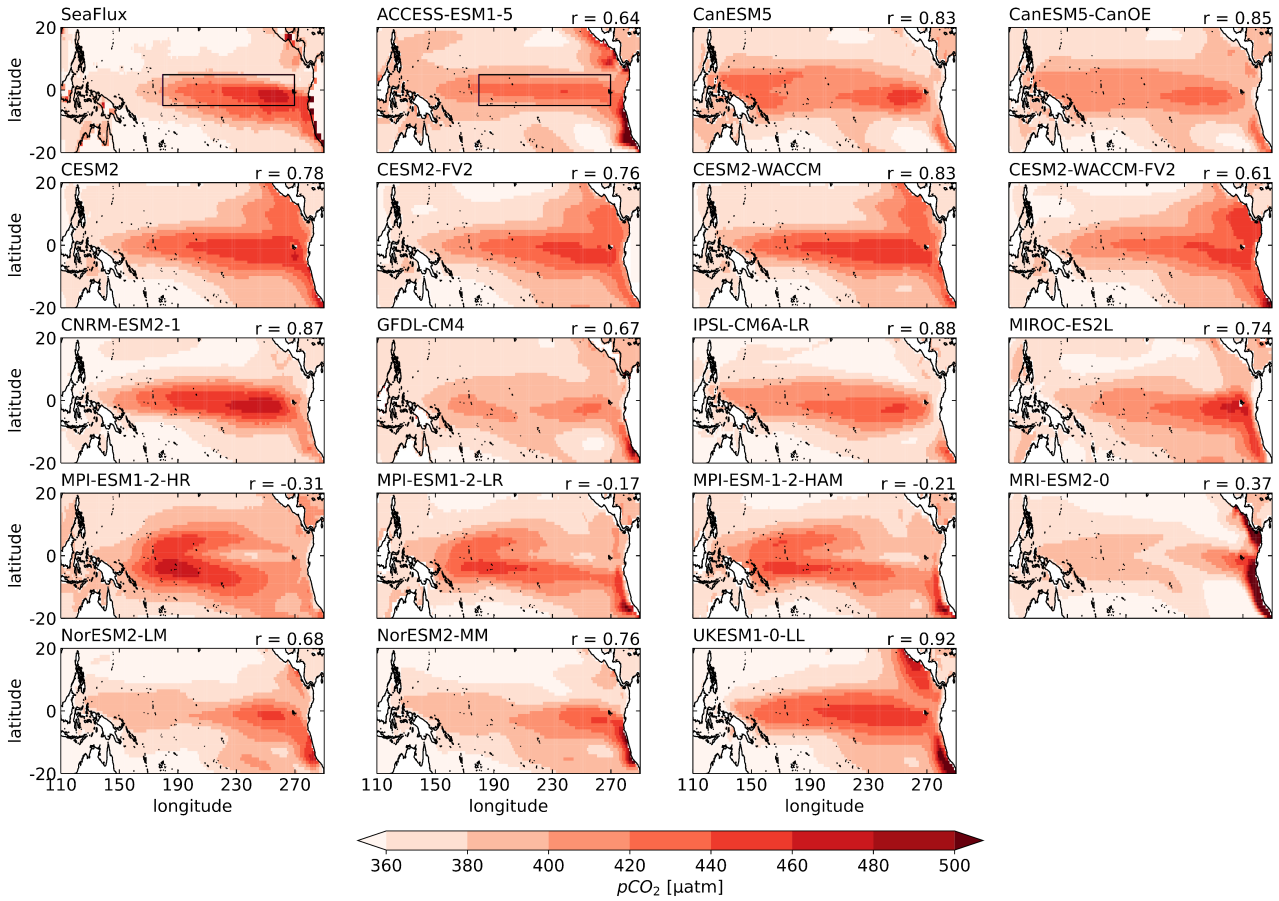

Figure S2. Tropical Pacific pCO_2 multi-year means from 1990-2014 (units: μatm) from the SeaFlux ensemble average (top left) and 18 CMIP6 models (other panels). Boxes in the SeaFlux and ACCESS-ESM1-5 panels mark the TPI region. The number (r) on the top right of each model's map is the SCC between the model and SeaFlux in the TPI region. Model multi-year means are evaluated using a single ensemble member per model.

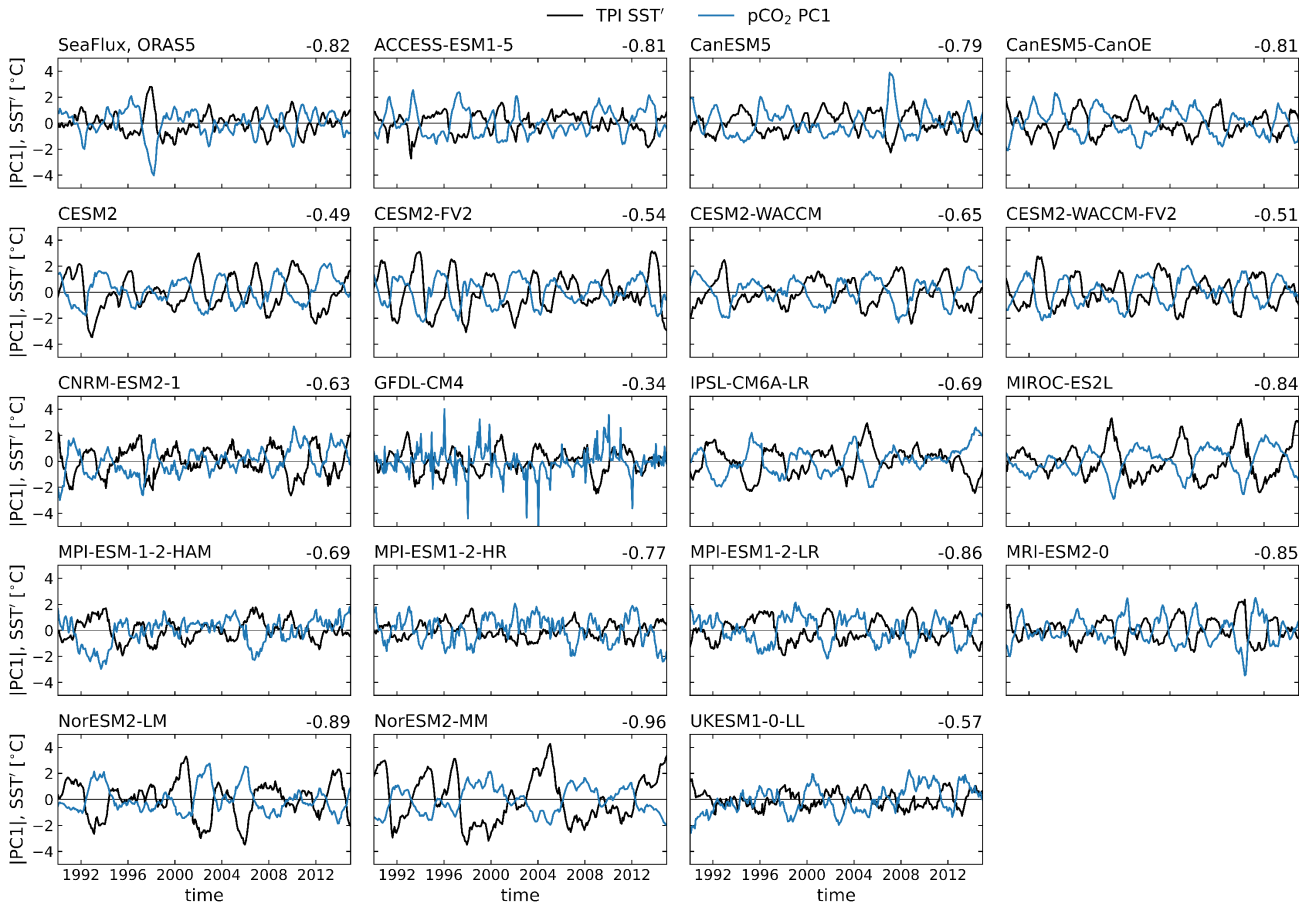

Figure S3. 1990-2014 time series of TPI SST anomalies (black lines) and the first principal component (PC1) of pCO_2 variability (blue lines) evaluated from ORAS5 and SeaFlux data, respectively (top-left). The other panels show the time series from 18 CMIP6 models. The correlation between TPI SST anomalies and pCO_2 PC1 are indicated by the number on the top-right of each panel.

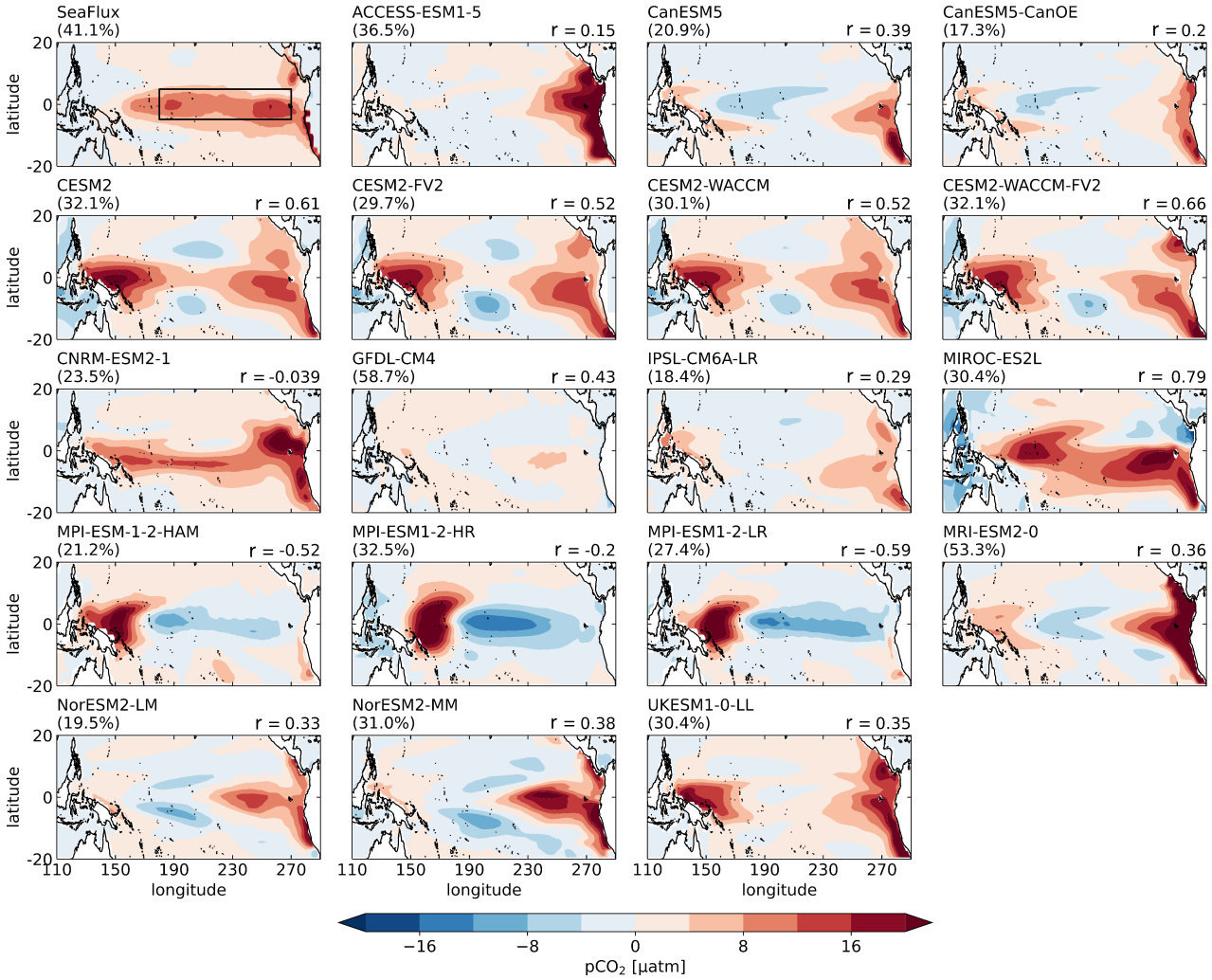

Figure S4. The first EOFs (units: μatm) of detrended pCO_2 anomalies in SeaFlux, averaged across the ensemble (top left), and 18 CMIP6 models (other panels). Model EOF patterns are calculated individually for each ensemble member before averaging over the ensemble. The percentage of the total variance in the tropical Pacific explained by EOF1 is given in parentheses above each panel. The number (r) on the top right of each model's panel is the SCC over the TPI region between each model's EOF1 and SeaFlux's EOF1. The TPI region is shown by the box in the top-left panel. The corresponding PC1 timeseries are shown in Figure S3.

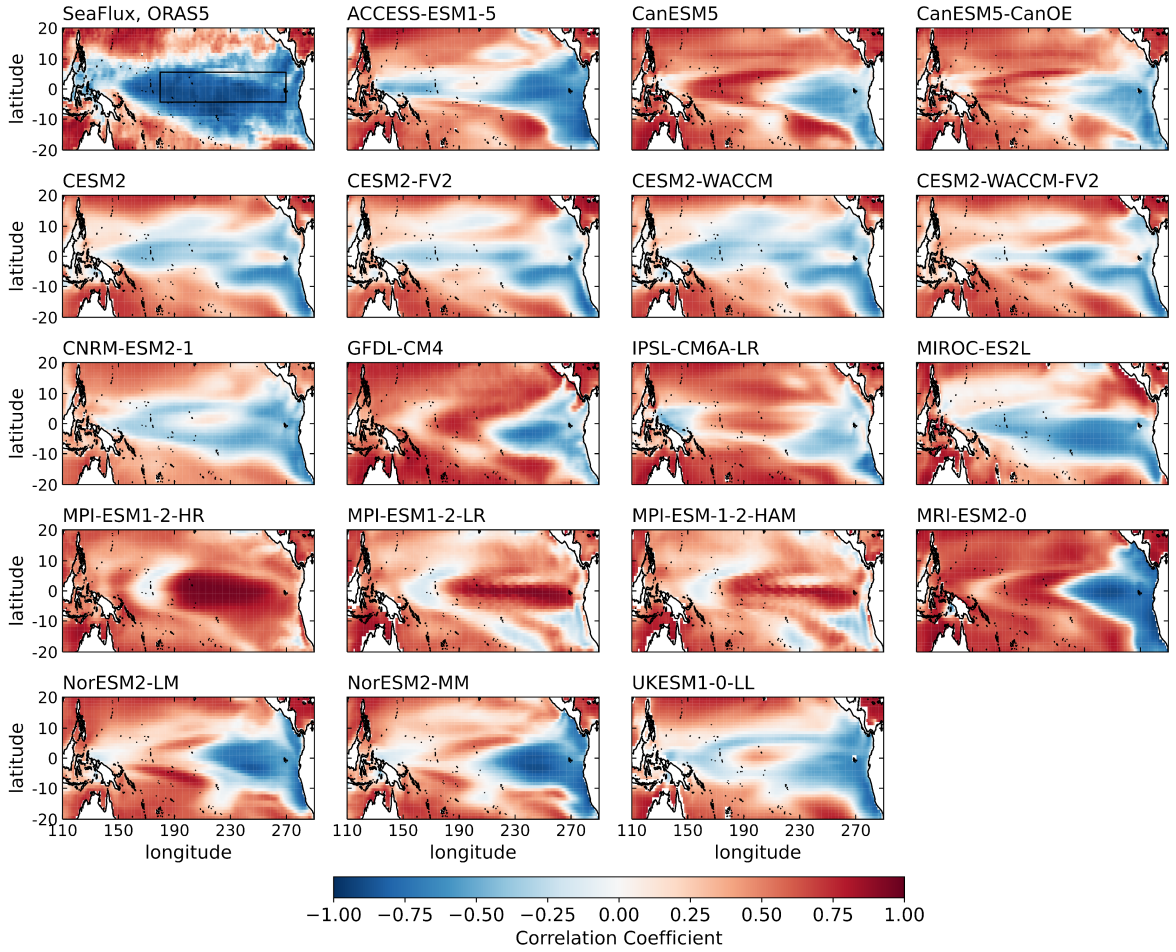

Figure S5. Correlation maps of detrended, pCO_2 and SST monthly anomalies over the tropical Pacific region. Time periods used: 1990-2014 for SeaFlux and ORAS5 (top-left), and 1959-2014 for models (other panels). Model correlation maps were calculated individually for each ensemble member before averaging over the ensemble. For the observations-based map, the mean across SeaFlux pCO_2 products was first taken before correlating with ORAS5 SSTs.

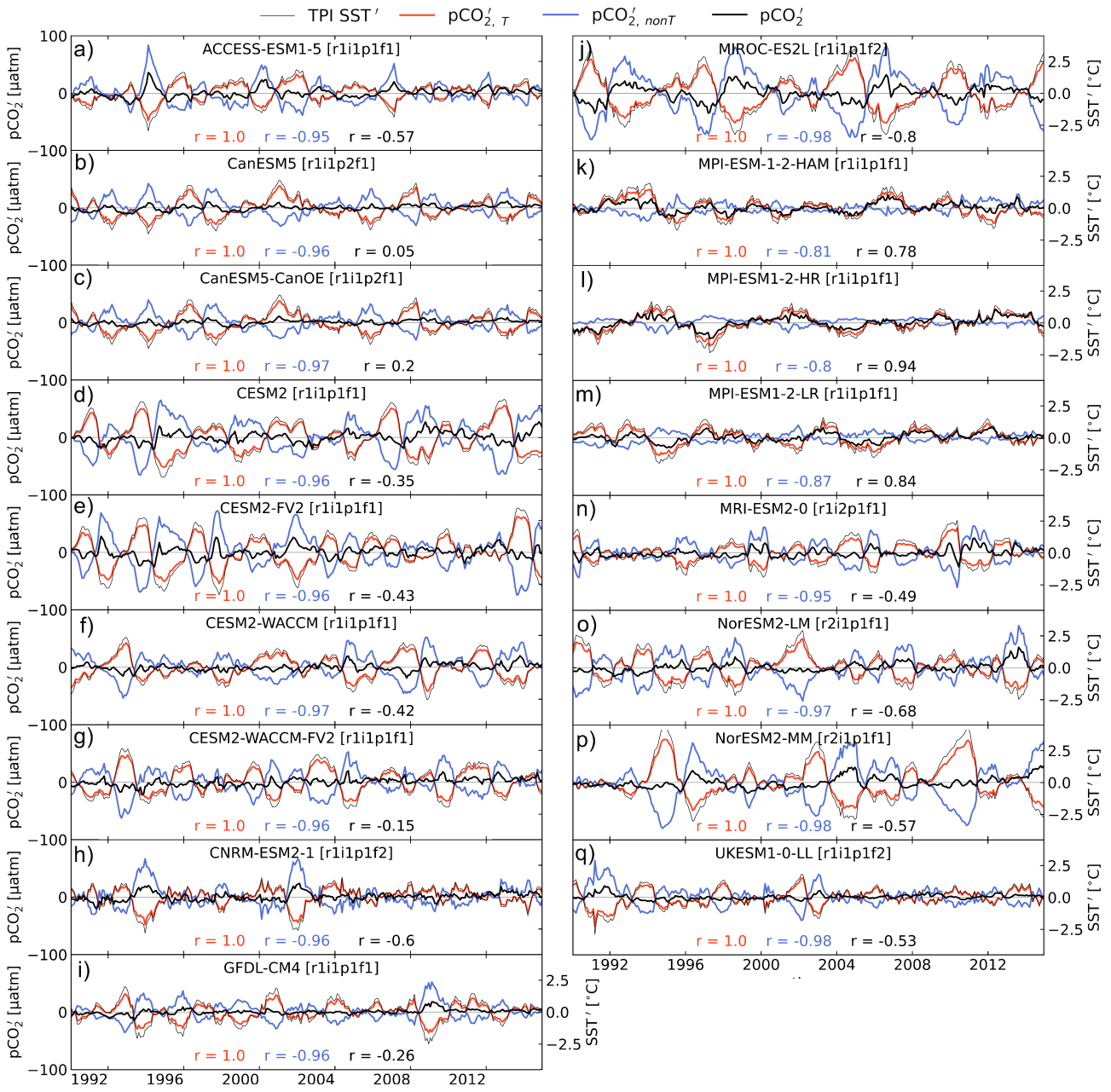

Figure S6. Thermal (red), non-thermal (blue), and total (bold black) pCO_2 anomalies (units: μatm) and TPI SST anomalies (thin black; units: $^{\circ}C$) over 1990-2014. Each panel (a through q) represents the time series from a single ensemble member from each CMIP6 model in this study. Correlation coefficients (r) between $pCO_{2,T}$, $pCO_{2,nonT}$ and total pCO_2 anomalies with TPI SST anomalies are shown in each panel in red, blue and black, respectively.

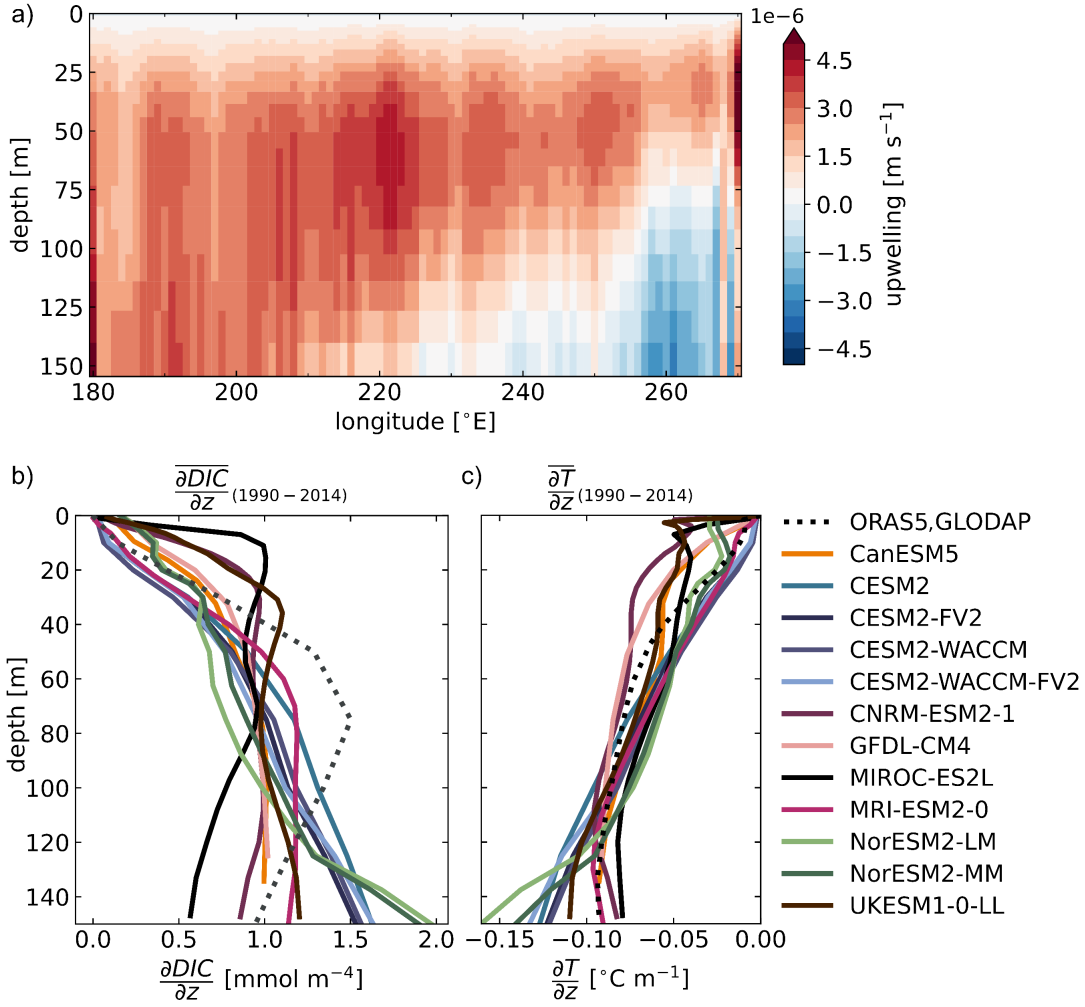

Figure S7. a) Time-averaged (1990-2014) upwelling section from ORAS5. The section was averaged between 5N to 5S. Positive values indicate upwelling (units: ms^{-1}). b) Vertical gradients of climatological DIC (units: $mmolm^{-4}$). GLODAPv2's DIC gradient is represented by the dashed black line. c) vertical gradients of climatological ocean temperatures (units: $°Cm^{-1}$). ORAS5's temperature gradient is represented by the dashed black line.

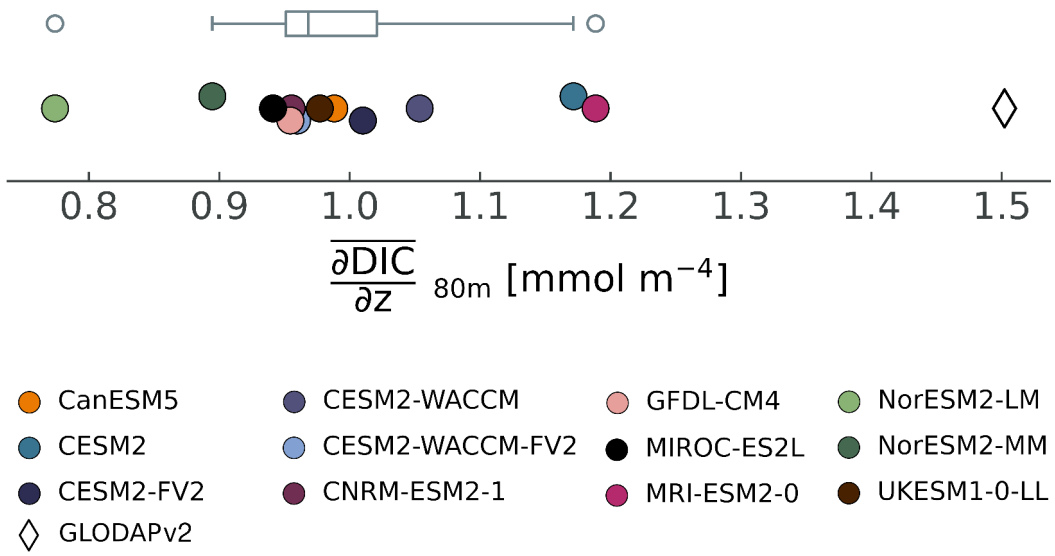

Figure S8. Amplitudes (units: mmolm^{-4}) of vertical gradients of climatological DIC, evaluated at 80m depth, across CMIP6 models (filled circles) versus GLODAPv2 (clear diamond). The boxplot represents the CMIP6 models.

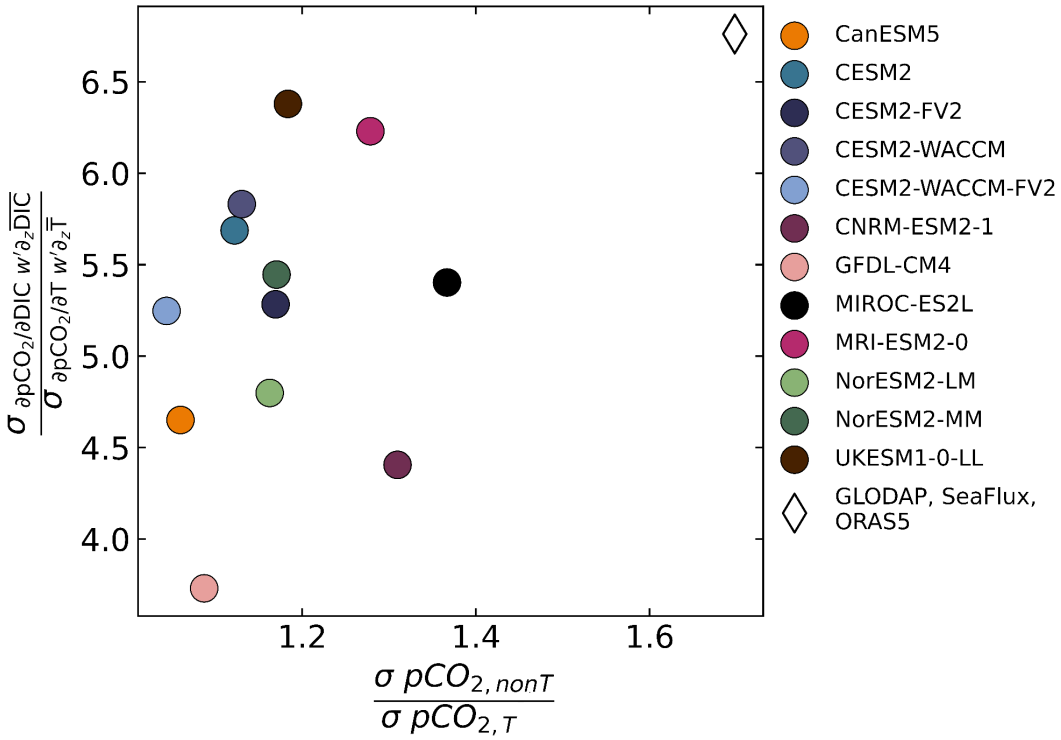

Figure S9. x-axis: Ratio of $pCO_{2,nonT}$ IAV to $pCO_{2,T}$ IAV (units: dimensionless). y-axis: Ratio of the vertical DIC gradients to the vertical temperature gradients at 50m depth, converted into units of pCO_2 tendency (ratio units: dimensionless). Models are marked by filled circles and the observations-based data are the marked by the clear diamond. Each model here is represented by one ensemble member.